On the Relationship of the Effective Mobility and Photoconductance Mobility in Organic Solar Cells - Supplementary Information

Joachim Vollbrecht[1*†], Nurlan Tokmoldin[1*], Bowen Sun[1], Elifnaz Saglamkaya[1], Lorena Perdigón-Toro[1], Seyed Mehrdad Hosseini[1], Jae Hoon Son[2], Han Young Woo[2], Safa Shoaee[1,3], and Dieter Neher[1]

[1]Institute of Physics and Astronomy, University of Potsdam, Potsdam, Germany.
[2]Department of Chemistry, Korea University, Seoul, Republic of Korea.
[3]Paul-Drude-Institut für Festkörperelektronik, Leibniz-Institut im Forschungsverbund Berlin e.V, Berlin, Germany.
[*]Corresponding authors. Email: vollbrecht@uni-potsdam.de; tokmoldin@uni-potsdam.de
[†]Current address: Institut für Solarenergieforschung GmbH, Emmerthal, Germany.

S1 Experimental Details

S1.1 Materials

In this study we consider systems with three donor polymers:
- Poly-(3-hexylthiophen-2,5-diyl) (P3HT);
- Poly[[4,8-bis[5-(2-ethylhexyl)-4-fluoro-2-thienyl]benzo[1,2-b:4,5-b']dithiophene-2,6-diyl]-2,5-thiophenediyl-[5,7-bis(2-ethylhexyl)-4,8-dioxo-4*H*,8*H*-benzo[1,2-c:4,5-c']dithiophene-1,3-diyl]-2,5-thiophenediyl] (PM6);
- Poly[(2,5-bis(2-hexyldecyloxy)phenylene)-alt-(5,6-difluoro-4,7-di(thiophen-2-yl)-benzo[c]-[1,2,5] thiadiazole)] (PPDT2FBT).

Furthermore, fullerene and non-fullerene acceptors were used:
- [6,6]-phenyl-C_{61}-butyricacidmethylester (P3HT:PC_{60}BM);
- 2,2'-((2*Z*,2'*Z*)-((12,13-bis(2-ethylhexyl)-3,9-diundecyl-12,13-dihydro-[1,2,5]thiadiazolo[3,4-e]thieno-[2",3":4',5']thieno[2',3':4,5]pyrrolo[3,2-g]thieno[2',3':4,5]thieno[3,2-b]indole-2,10-diyl)bis(methanylylidene))-bis(3-oxo-2,3-dihydro-1*H*-indene-2,1-diylidene))dimalononitrile (Y5);
- 2,2'-((2*Z*,2'*Z*)-((12,13-bis(2-ethylhexyl)-3,9-diundecyl-12,13-dihydro-[1,2,5]thiadiazolo[3,4-e]thieno-[2",3":4',5']thieno[2',3':4,5]pyrrolo[3,2-g]thieno[2',3':4,5]thieno[3,2-b]indole-2,10-diyl)bis(methanylylidene))-bis(5,6-difluoro-3-oxo-2,3-dihydro-1*H*-indene-2,1-diylidene))dimalononitrile (Y6);

- 2,2'-((2*Z*,2'*Z*)-((6,12,13-tris(2-ethylhexyl)-3,9-diundecyl-12,13-dihydro-6*H*-thieno[2",3":4',5']thieno-[2',3':4,5]pyrrolo[3,2-g]thieno[2',3':4,5]thieno[3,2-b][1,2,3]triazolo[4,5-e]indole-2,10-diyl)bis(methanylylidene))-bis(5,6-difluoro-3-oxo-2,3-dihydro-1*H*-indene-2,1-diylidene))dimalononitrile (Y11);
- 2,2'-((2*Z*,2'*Z*)-((12,13-bis(4-ethyloctyl)-3,9-diundecyl-12,13-dihydro-[1,2,5]thiadiazolo[3,4-e]thieno-[2",3":4',5']thieno[2',3':4,5]pyrrolo[3,2-g]thieno[2',3':4,5]thieno[3,2-b]indole-2,10-diyl)bis(methanylylidene))-bis(5,6-difluoro-3-oxo-2,3-dihydro-1*H*-indene-2,1-diylidene))dimalononitrile (N4);
- 2,2'-((2*Z*,2'*Z*)-((6-(2-ethylhexyl)-12,13-bis(4-ethyloctyl)-3,9-diundecyl-12,13-dihydro-6*H*-thieno-[2",3":4',5']thieno[2',3':4,5]pyrrolo[3,2-g]thieno-[2',3':4,5]thieno[3,2-b]triazolo[4,5-e]indole-2,10-diyl)-bis(methanylylidene))bis(5,6-difluoro-3-oxo-2,3-dihydro-1*H*-indene-2,1-diylidene))dimalononitrile (Y11-N4).

S1.2 Device Fabrication

A variety of organic photovoltaic (OPV) solar cells employed for the study were fabricated on indium-tin oxide (ITO)-coated pre-etched and pre-cleaned glass substrates. In all OPV devices, a 30-nm-thick poly(3,4-ethylenedioxythiophene) polystyrene sulfonate (PEDOT:PSS) film was used as a hole-transporting layer (HTL). Active layer solutions were spin-coated by varying spin speeds and accelerations to obtain the desired thicknesses. The weight ratios of a donor to acceptor for the different blend systems employed in this study were as follows: P3HT:$PC_{60}BM$ – 1:1, PM6:Y11-N4 – 1:1.3, PM6:Y5 – 1:1.2, PPDT2FBT:Y6 – 1:2, PM6:Y11 – 1:1, PM6:N4 – 1:1.25, PM6:Y6 – 1:1.2. The PM6:Y6 solar cells included a chloronaphthalene (CN) solvent additive in the amount of 0.5% by volume. Active layer annealing was performed at the following conditions: PM6 and PPDT2FBT-based NFA devices at 110°C for 10 min. For the PM6 and PPDT2FBT-based NFA cells, a 10-nm-thick PDINO electron-injecting layer (ETL) was spin-cast, whereas a 10-nm-thick PDINN ETL was spin-cast instead of PDINO for one of the PM6:Y6 devices. Finally, thermal evaporation was employed to deposit the Ag-electrode (45 nm in case of the PM6:N4 and PM6:Y11-N4 devices, 100 nm for all the other devices).

S1.3 Device Characterization

Current-voltage (J-V): *J-V* measurements of the studied solar cells were performed using a LabVIEW-controlled Keithley 2400 SourceMeter under the illumination of a white-light LED array.
Impedance: The impedance measurements were performed using a Keysight E5061B Vector Network Analyser in the frequency range from 50 Hz to 10 MHz under the illumination of a white-light LED array. The 85032E Type N kit was used for the instrument calibration, and the presence of the test fixture was compensated for using the "Open," "Short," and "50 Ohm" measurements. Capacitance-frequency spectra of the studied solar cells were generated from the impedance measurements at various light intensities and applied biases (cf. Fig. S11 - S19). The integration of the

capacitance over the voltage range yields the charge carrier density n:

$$n = \frac{1}{qAL} \int_{V_{\mathrm{sat}}}^{V_{\mathrm{OC}}} [C_{\mathrm{b}} - C_{\mathrm{g}}] \, \mathrm{d}V_{\mathrm{cor}}, \tag{S1}$$

where q is the elementary charge, A is the device area, L is the active layer thickness, V_{sat} is the saturated voltage (usually $V_{\mathrm{sat}} \leq 0$ V), C_{b} is the frequency dependent barrier capacitance obtained via the impedance measurements, C_{g} is the geometric capacitance resulting from the electrodes of the device forming a plate capacitor, and V_{cor} is the voltage corrected for the series resistance R_{series}. More details related to this technique can be found in Ref. [1].

Quasi-steady state photoconductance: Quasi-steady state photoconductance of the devices under illumination was determined at the respective open-circuit conditions using the real part of admittance $Y = 1/Z$ averaged across the lower-frequency range of 50 Hz to 1 kHz, in which conductance varies insignificantly.[2]

Space-charge limited current (SCLC): SCLC measurements were performed similar to the J-V measurements in the dark on single-carrier diodes using either an ITO/PEDOT:PSS - MoO_3/Ag electrode combination for hole-only devices, or an ITO/ZnO - PDINO/Ag electrode combination for electron-only devices. Mobilities were determined via drift-diffusion fitting using a previously reported open-source software.[3]

S2 Optoelectronic Characterization

S2.1 Overview of Mobility Results

In this study, nine different organic solar cells were investigated over a wide range of light intensities. Namely, solar cells based on P3HT:$PC_{60}BM$, PM6:Y11-N4, PM6:Y5, PPDT2FBT:Y6, PM6:Y11, PM6:N4, and PM6:Y6, the latter with varying electron transport layers and thicknesses, were fabricated (cf. Fig. S1).

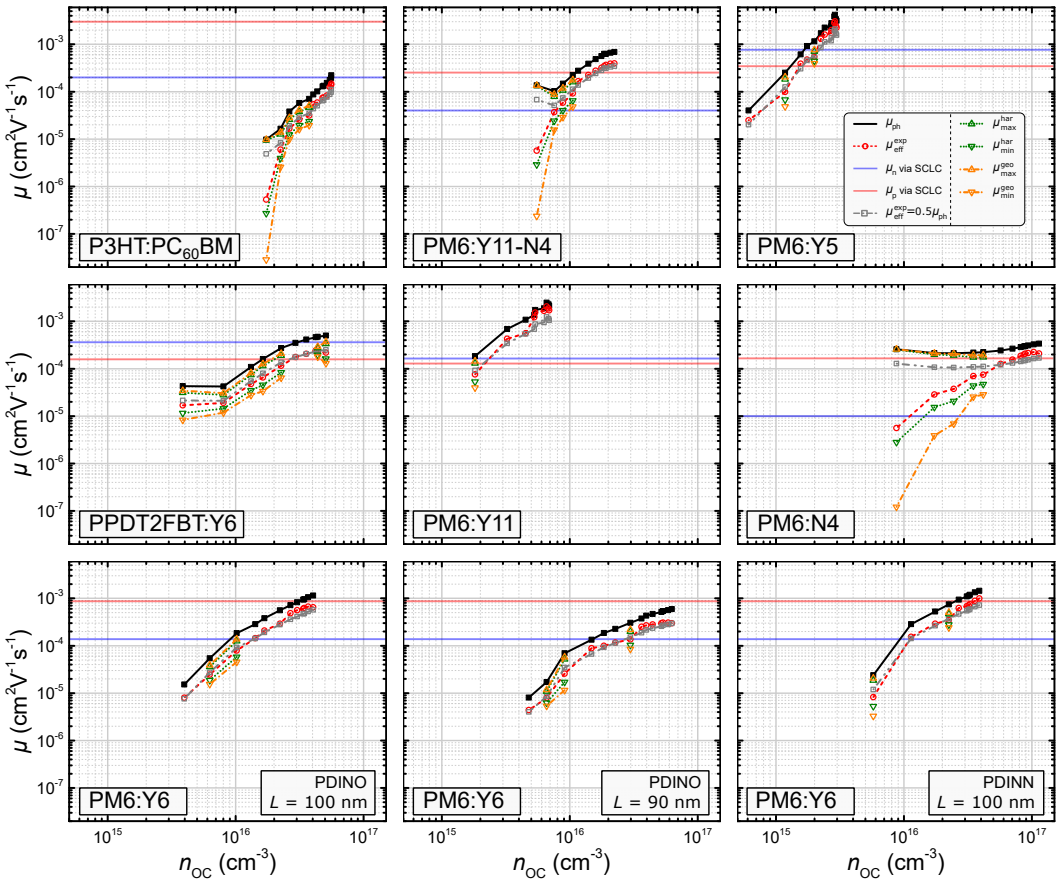

Figure S1: Experimentally determined values for μ_{ph} (black squares; cf. Eq. 4 in the main manuscript) and $\mu_{\mathrm{eff}}^{\mathrm{exp}}(V_{\mathrm{OC}})$ (red circles; cf. Eq. 3 in the main manuscript) for various organic solar cells. Calculation of the maximum and minimum mobilities determined via the harmonic and geometric approach ($\mu_{\mathrm{max}}^{\mathrm{har}}$, $\mu_{\mathrm{min}}^{\mathrm{har}}$: green dots, cf. Eq. 8 and Eq. 9 in the main manuscript; $\mu_{\mathrm{max}}^{\mathrm{geo}}$, $\mu_{\mathrm{min}}^{\mathrm{geo}}$: orange dash-dots, cf. Eq. 11 and Eq. 12 in the main manuscript) and for the relationship $\mu_{\mathrm{eff}}^{\mathrm{exp}} = 0.5 \cdot \mu_{\mathrm{ph}}$ (gray squares; cf. Eq. 6 in the main manuscript). The horizontal lines show the electron (μ_{n}: blue) and hole (μ_{p}: red) mobilities determined via the SCLC method of single carrier diodes. These mobilities are shown as horizontal lines due to the unknown charge carrier density at which they were measured.

S2.2 J-V-Characteristics

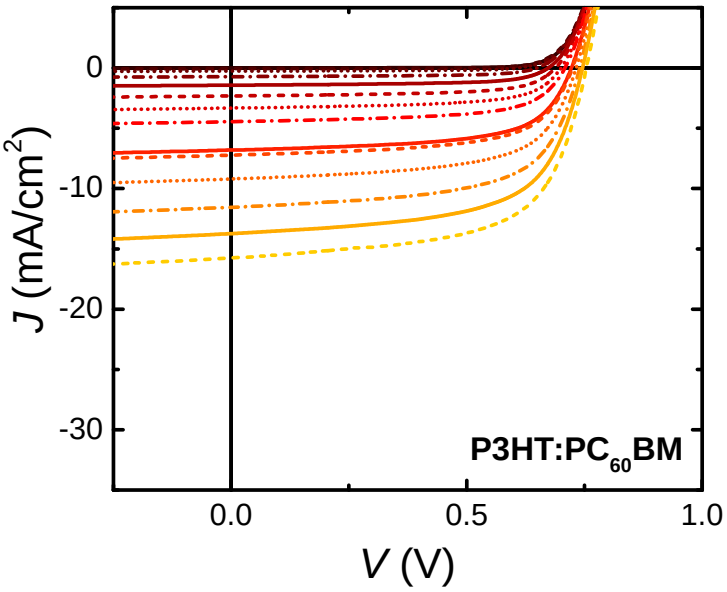

Figure S2: Current-density-voltage characteristics of a P3HT:$PC_{60}BM$ solar cell at different light intensities (black: dark; yellow: increasing light intensity).

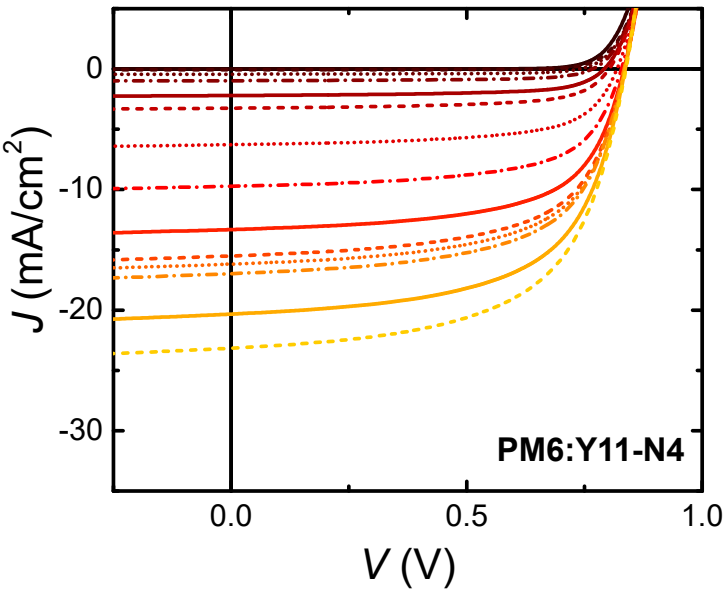

Figure S3: Current-density-voltage characteristics of a PM6:Y11-N4 solar cell at different light intensities (black: dark; yellow: increasing light intensity).

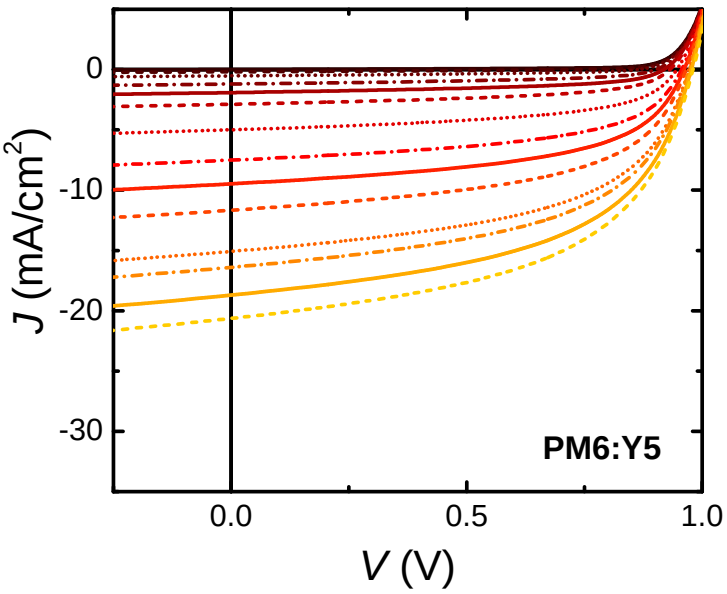

Figure S4: Current-density-voltage characteristics of a PM6:Y5 solar cell at different light intensities (black: dark; yellow: increasing light intensity).

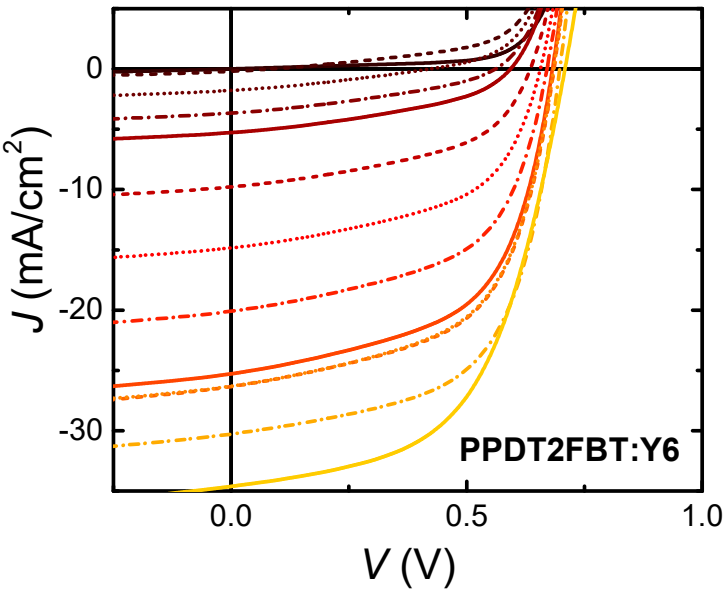

Figure S5: Current-density-voltage characteristics of a PPDT2FBT:Y6 solar cell at different light intensities (black: dark; yellow: increasing light intensity).

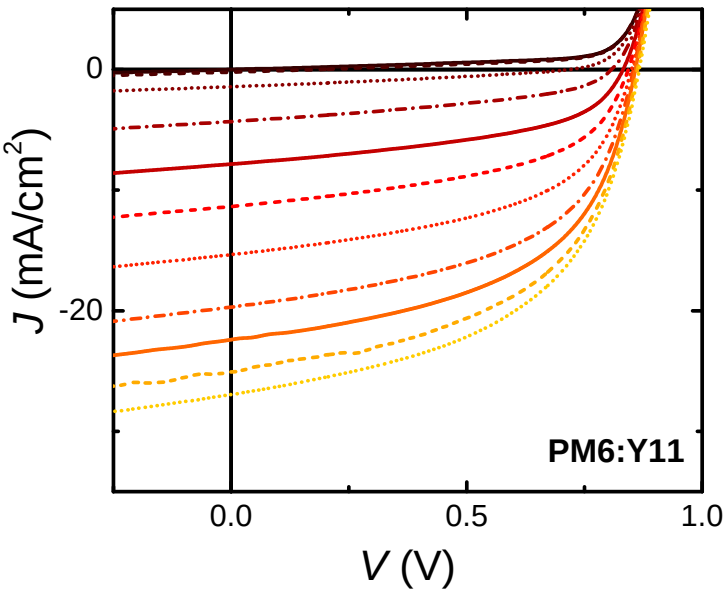

Figure S6: Current-density-voltage characteristics of a PM6:Y11 solar cell at different light intensities (black: dark; yellow: increasing light intensity).

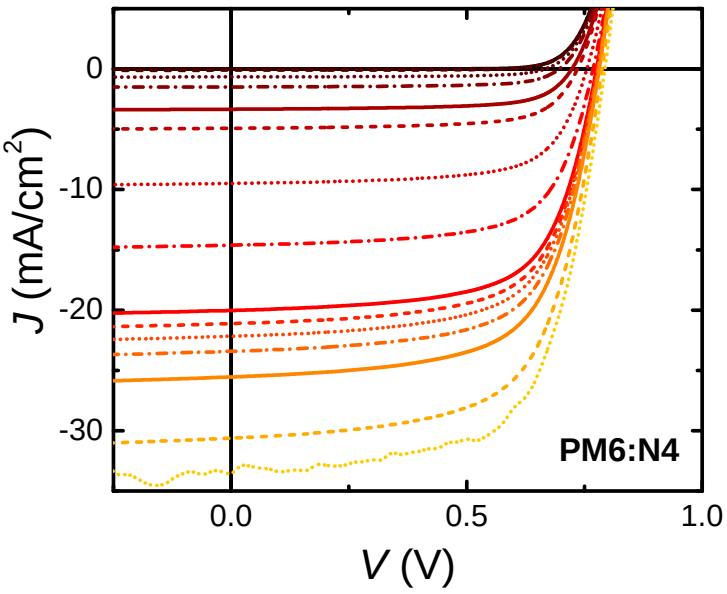

Figure S7: Current-density-voltage characteristics of a PM6:N4 solar cell at different light intensities (black: dark; yellow: increasing light intensity).

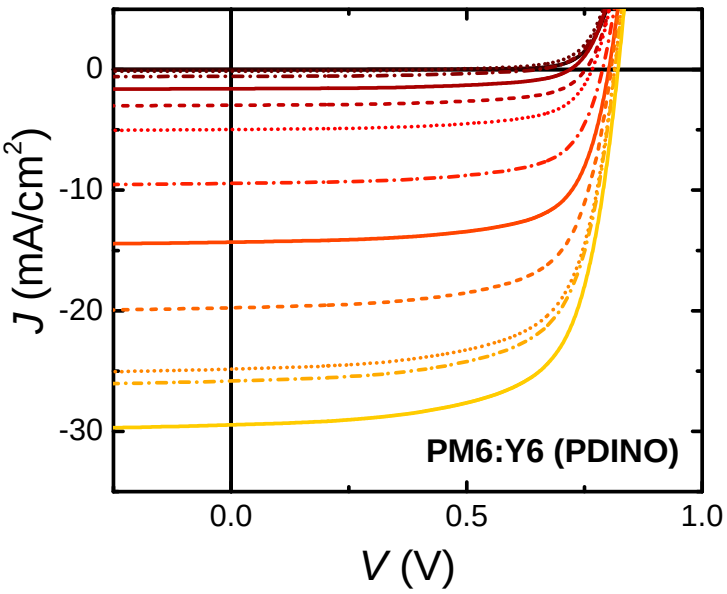

Figure S8: Current-density-voltage characteristics of a PM6:Y6 (PDINO; $L = 100$ nm) solar cell at different light intensities (black: dark; yellow: increasing light intensity).

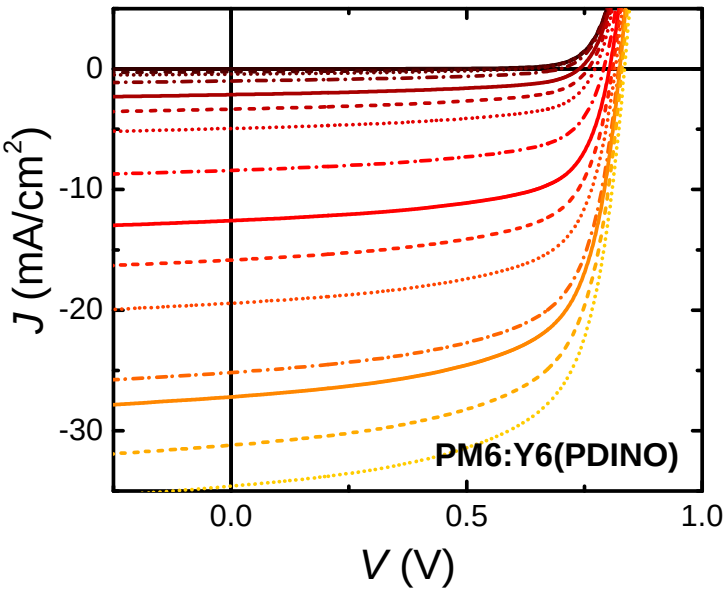

Figure S9: Current-density-voltage characteristics of a PM6:Y6 (PDINO; $L = 90$ nm) solar cell at different light intensities (black: dark; yellow: increasing light intensity).

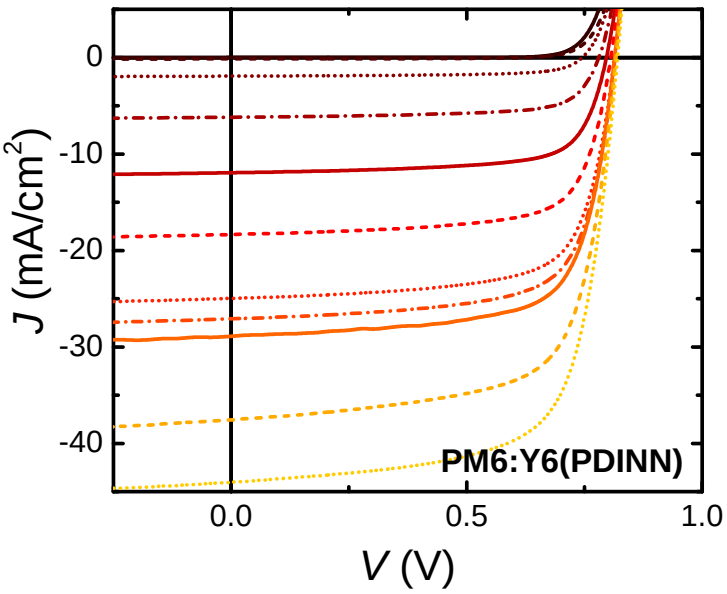

Figure S10: Current-density-voltage characteristics of a PM6:Y6 (PDINN; $L = 100$ nm) solar cell at different light intensities (black: dark; yellow: increasing light intensity).

S2.3 Capacitance Spectra

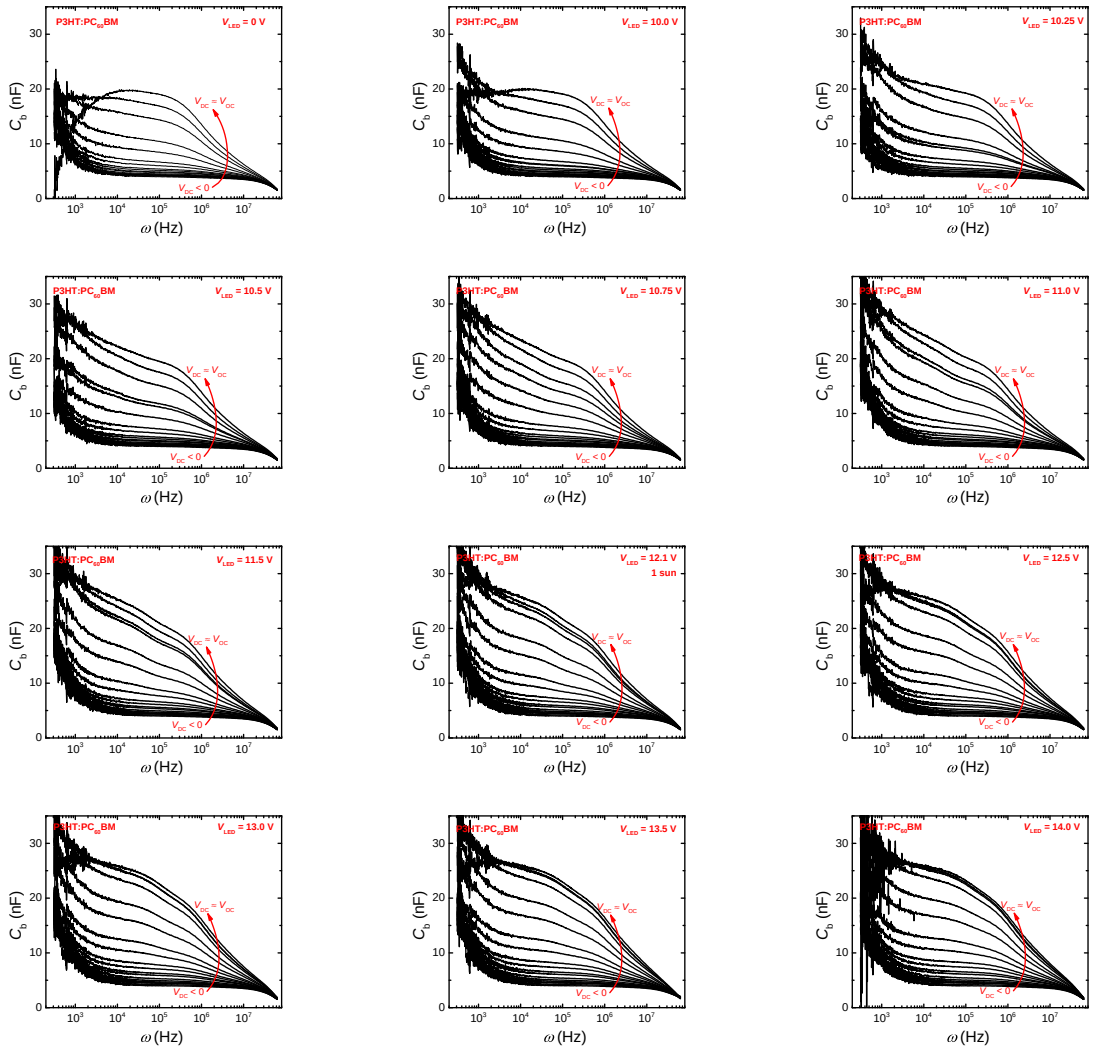

Figure S11: Frequency dependent barrier capacitance C_b at different light intensities (V_LED) and DC-voltages (V_DC) of a P3HT:PC$_{60}$BM solar cell.

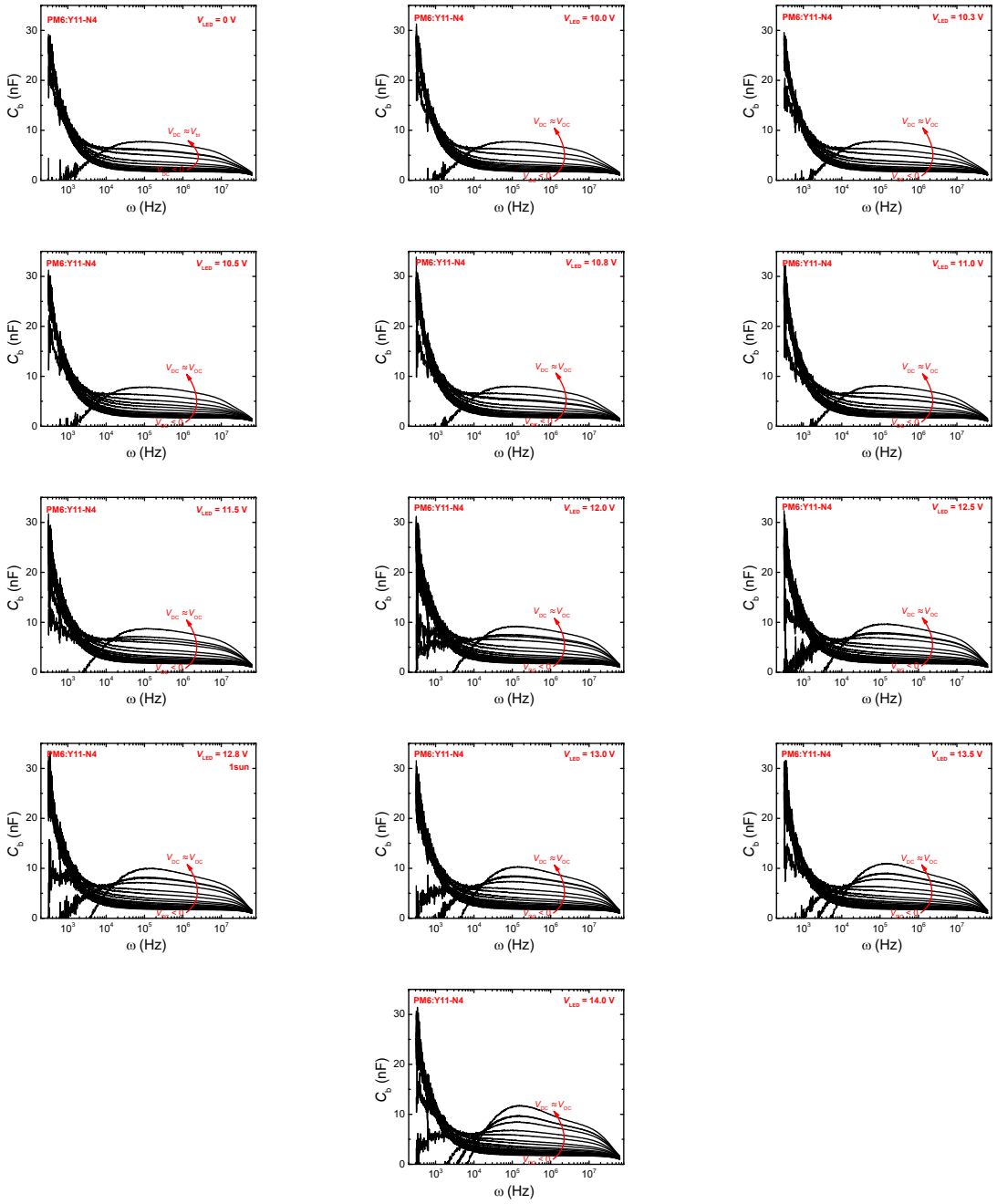

Figure S12: Frequency dependent barrier capacitance C_{b} at different light intensities (V_{LED}) and DC-voltages (V_{DC}) of a PM6:Y11-N4 solar cell.

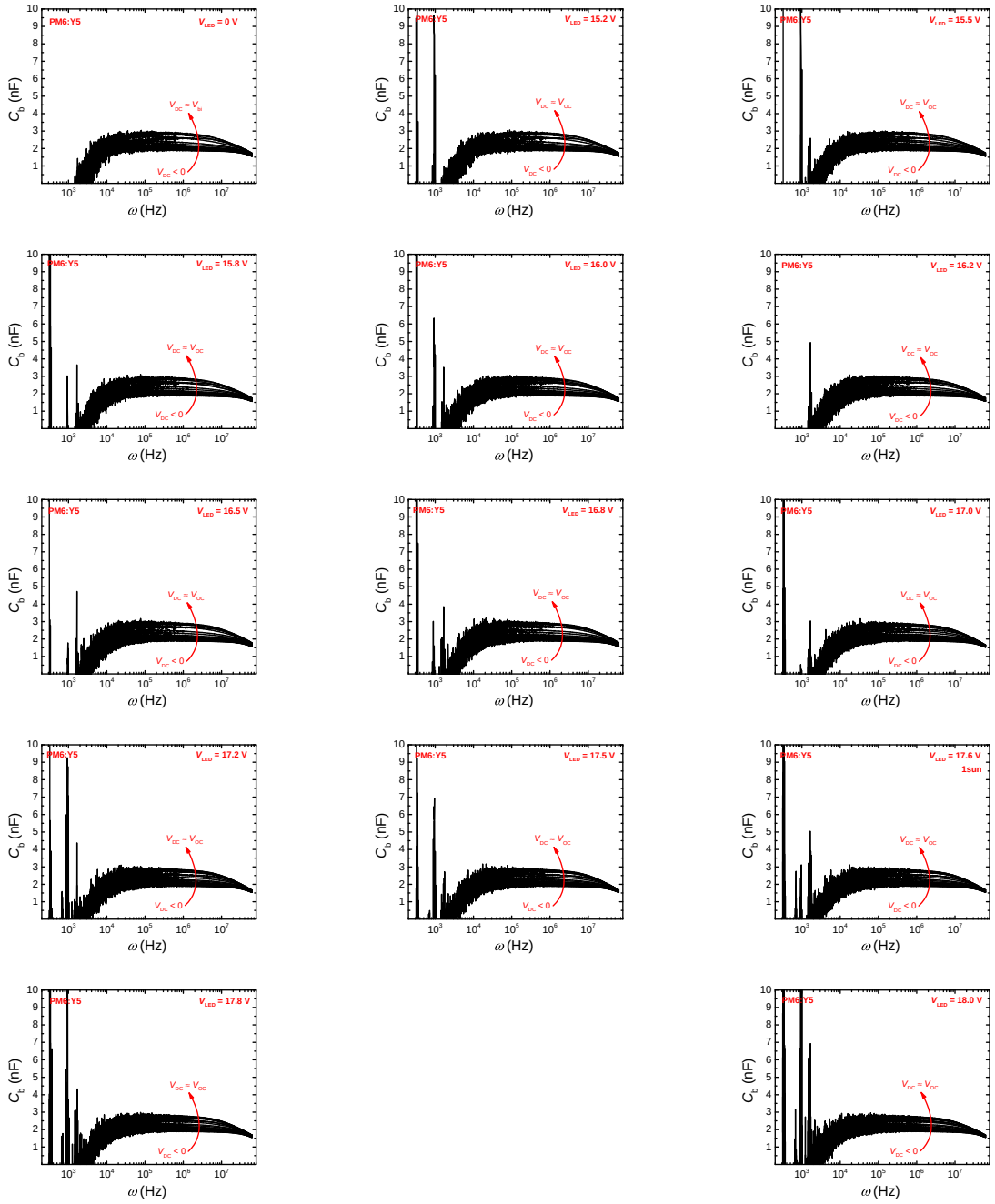

Figure S13: Frequency dependent barrier capacitance C_{b} at different light intensities (V_{LED}) and DC-voltages (V_{DC}) of a PM6:Y5 solar cell.

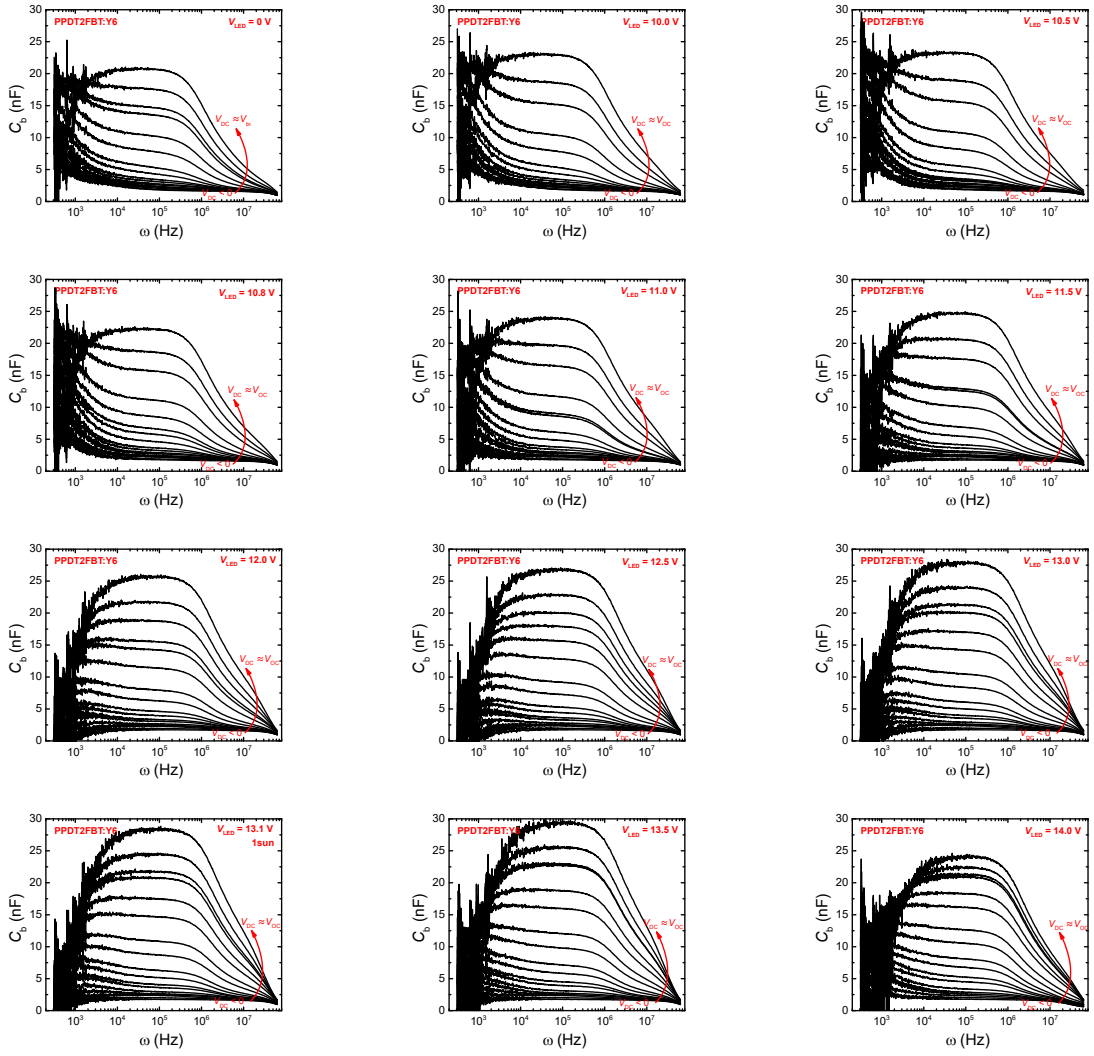

Figure S14: Frequency dependent barrier capacitance C_{b} at different light intensities (V_{LED}) and DC-voltages (V_{DC}) of a PPDT2FBT:Y6 solar cell.

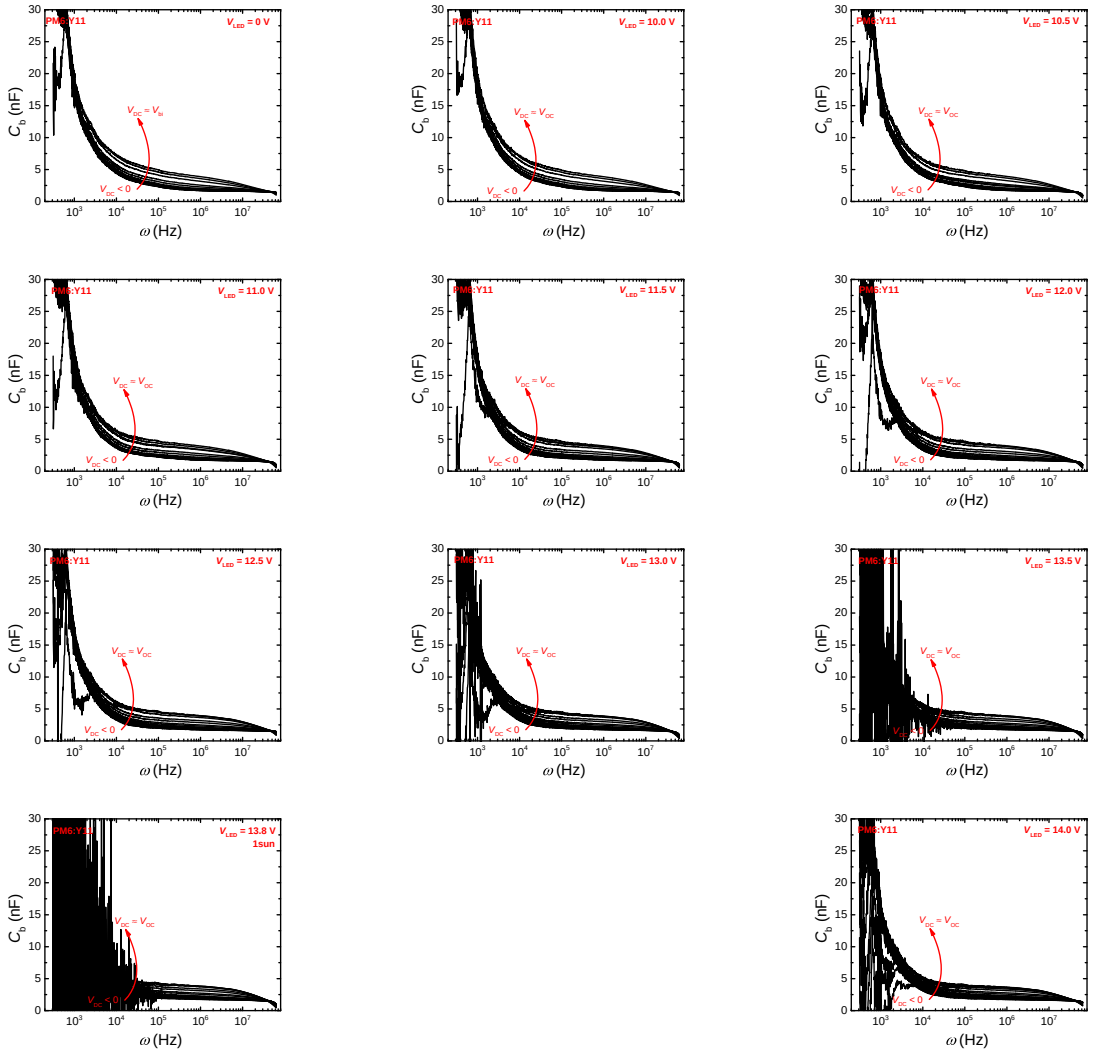

Figure S15: Frequency dependent barrier capacitance C_b at different light intensities (V_LED) and DC-voltages (V_DC) of a PM6:Y11 solar cell.

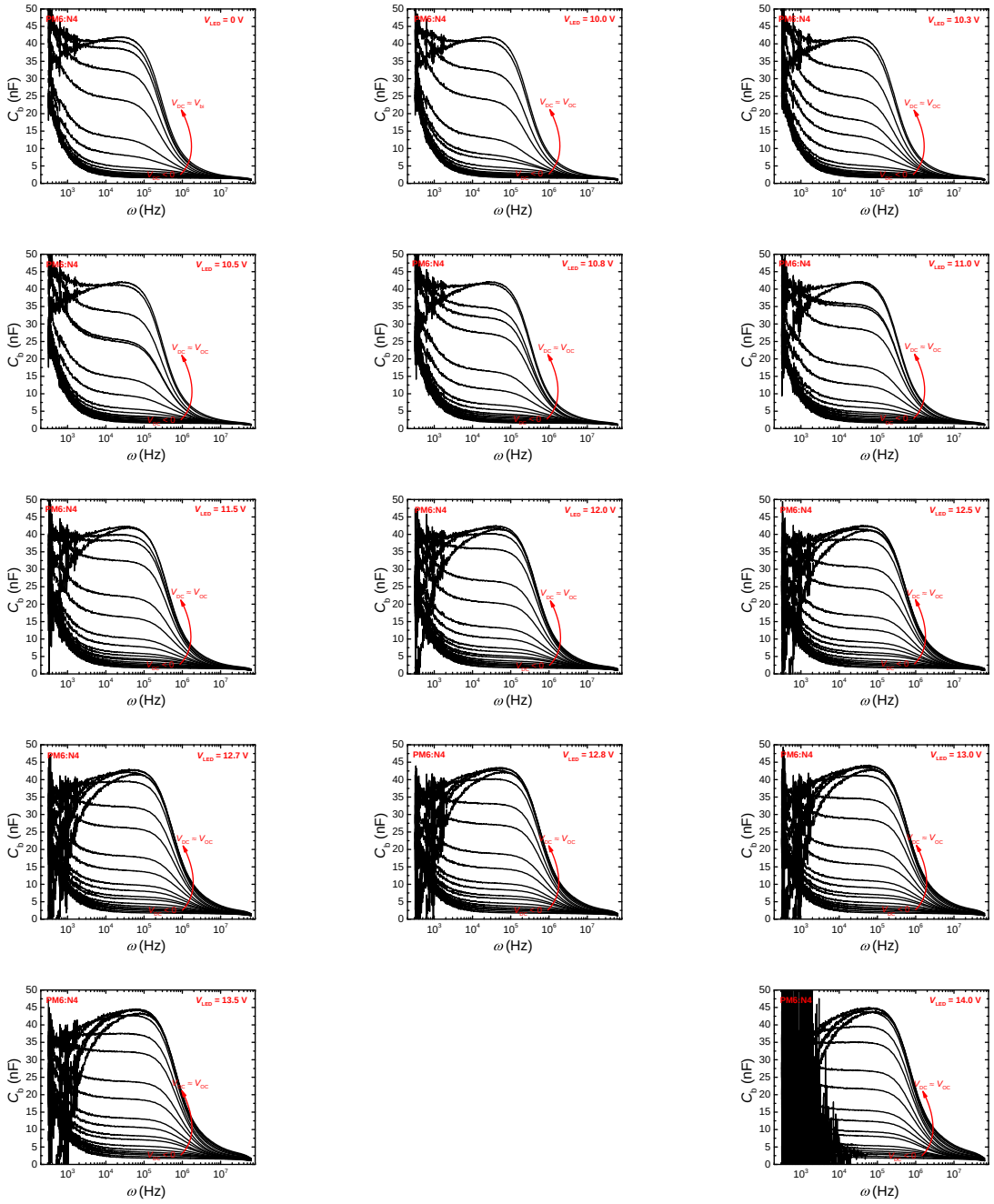

Figure S16: Frequency dependent barrier capacitance C_b at different light intensities (V_LED) and DC-voltages (V_DC) of a PM6:N4 solar cell.

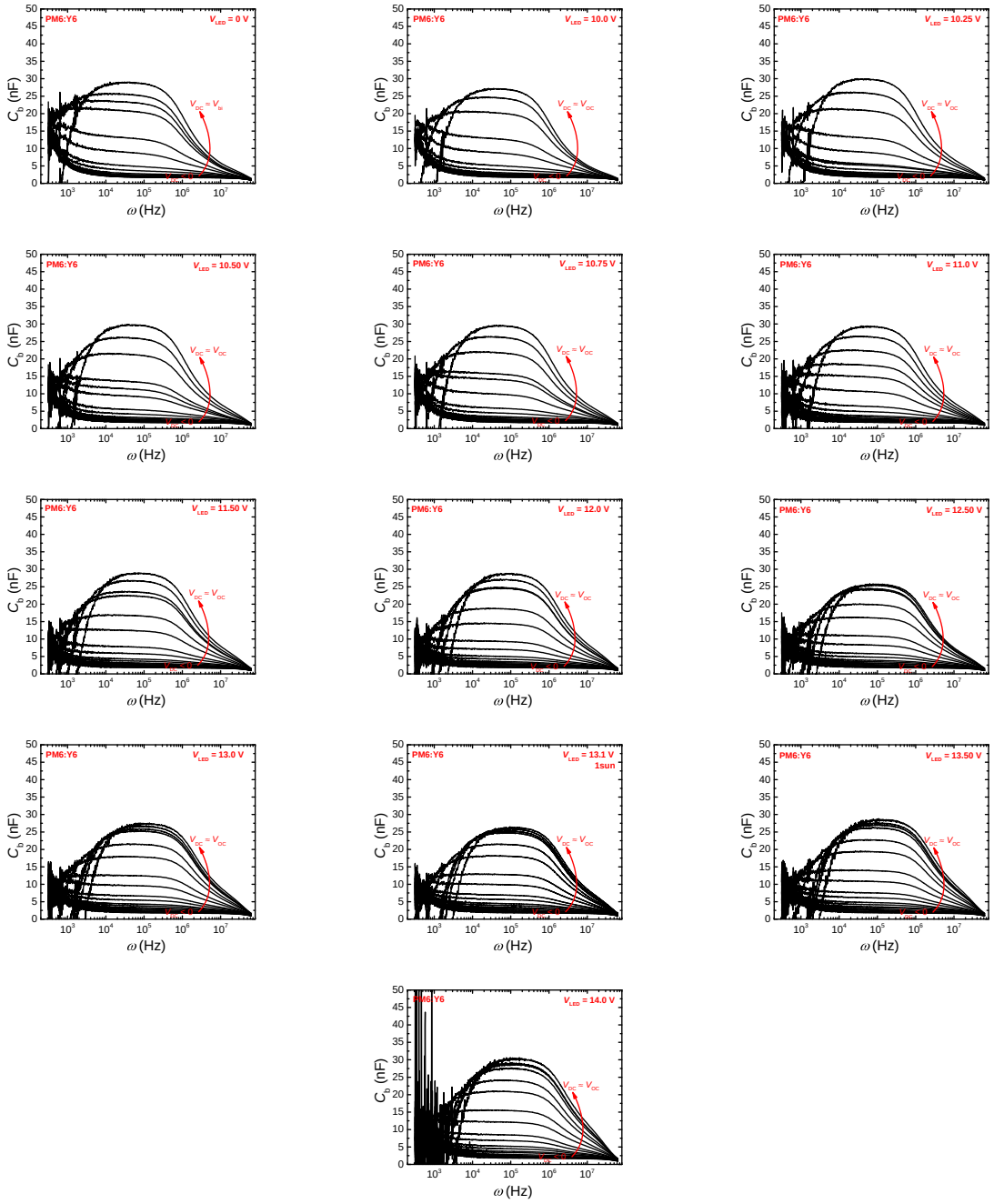

Figure S17: Frequency dependent barrier capacitance C_{b} at different light intensities (V_{LED}) and DC-voltages (V_{DC}) of a PM6:Y6 (PDINO; $L = 100$ nm) solar cell.

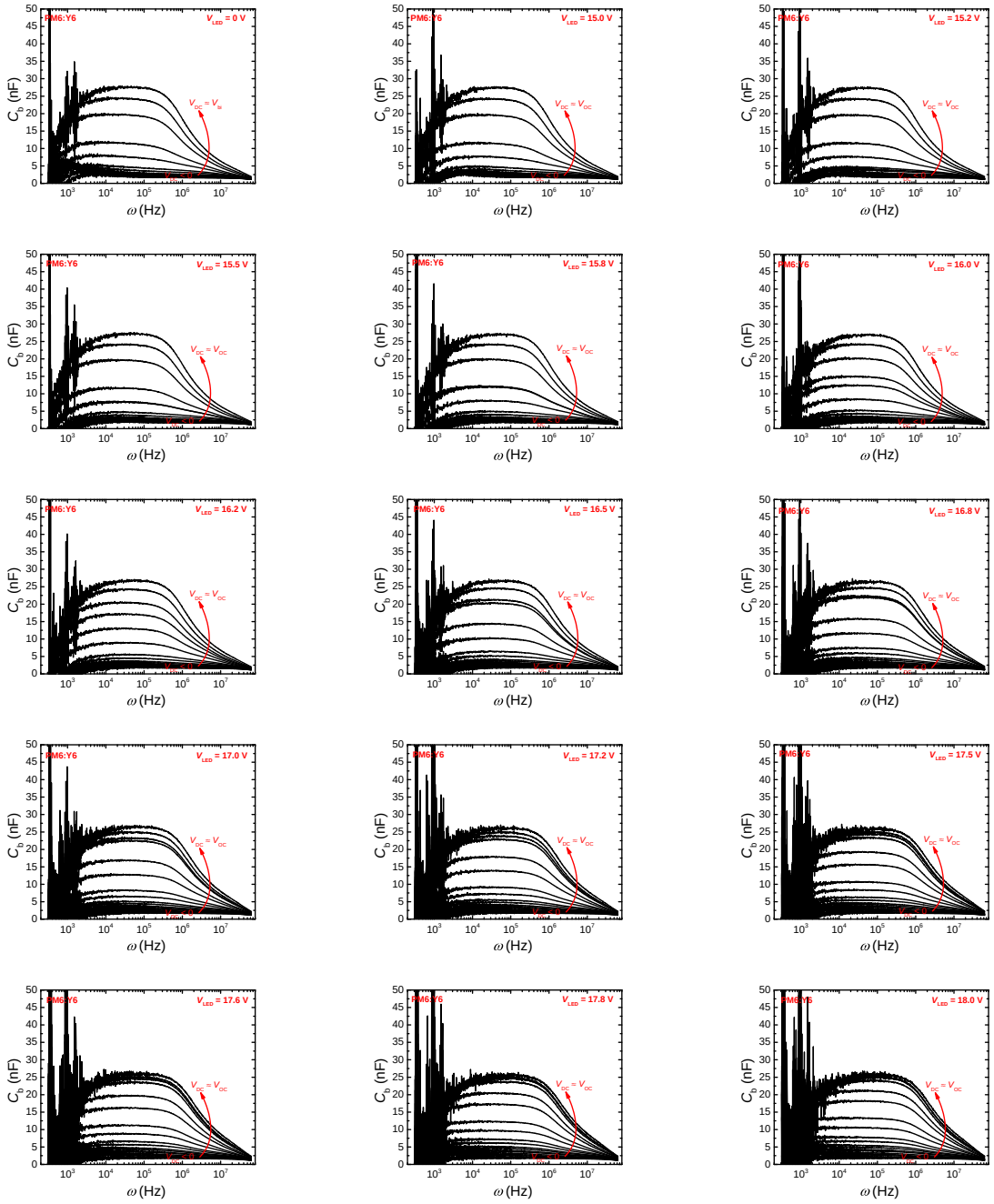

Figure S18: Frequency dependent barrier capacitance C_{b} at different light intensities (V_{LED}) and DC-voltages (V_{DC}) of a PM6:Y6 (PDINO; $L = 90$ nm) solar cell.

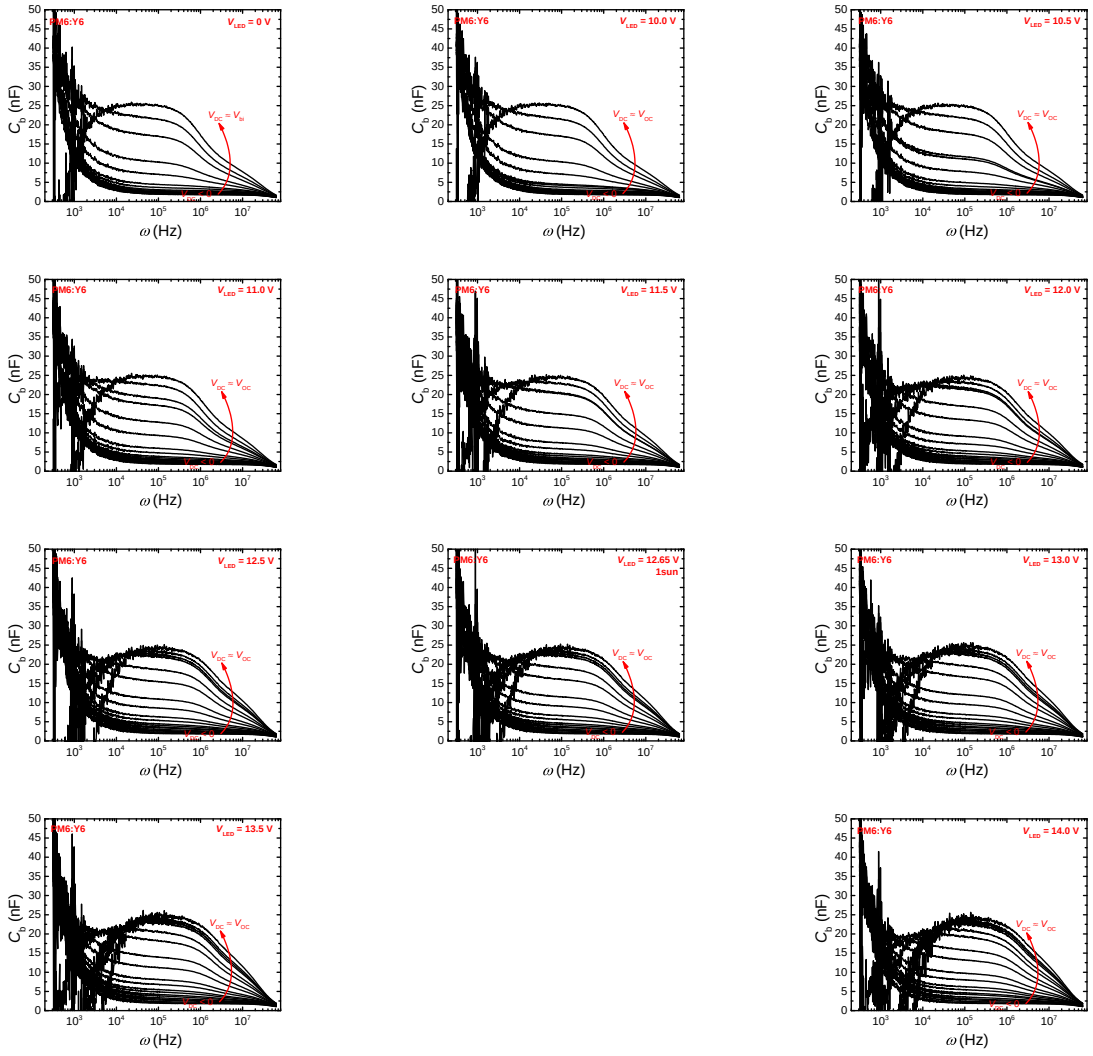

Figure S19: Frequency dependent barrier capacitance C_{b} at different light intensities (V_{LED}) and DC-voltages (V_{DC}) of a PM6:Y6 (PDINN; $L = 100$ nm) solar cell.

S2.4 SCLC-Analysis for the Reference Mobilities

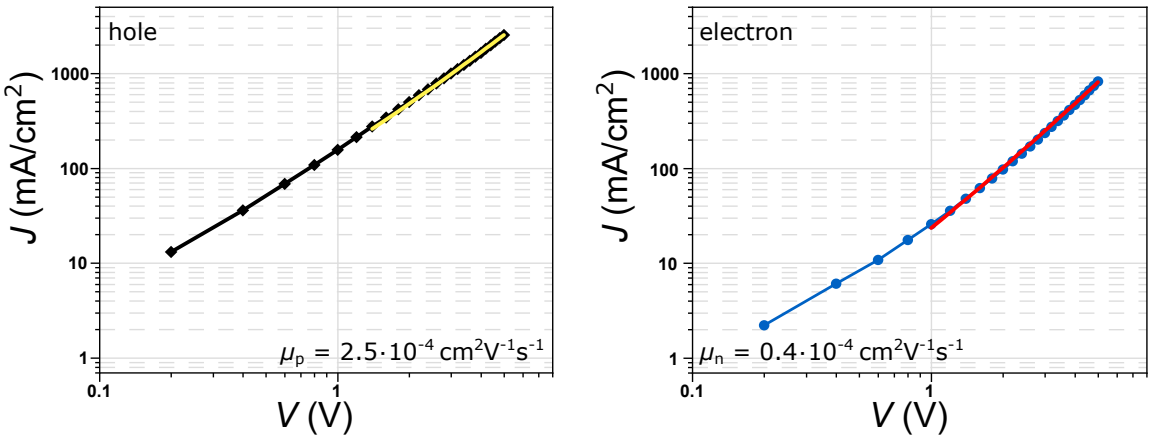

Figure S20: SCLC-plots of PM6:Y11-N4 hole and electron only diodes.

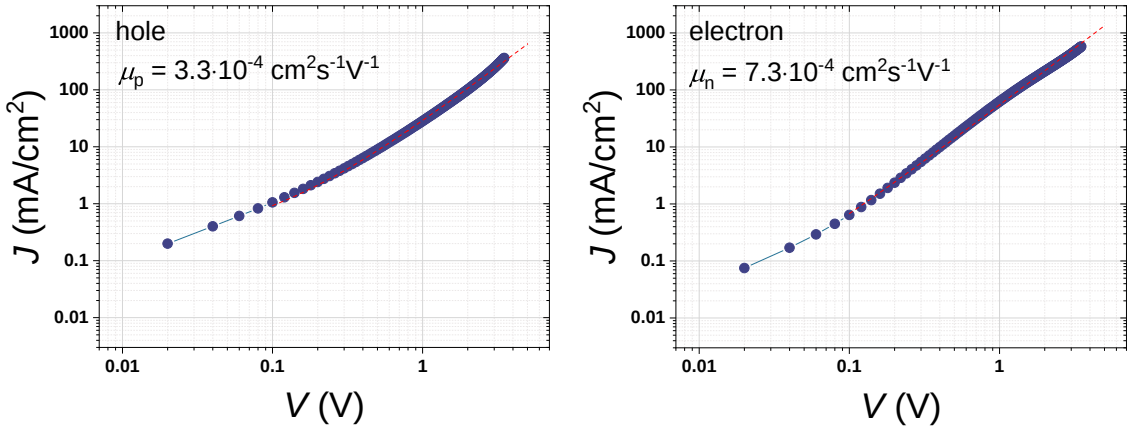

Figure S21: SCLC-plots of PM6:Y5 hole and electron only diodes. Both diodes have a 100 nm thick active layer.

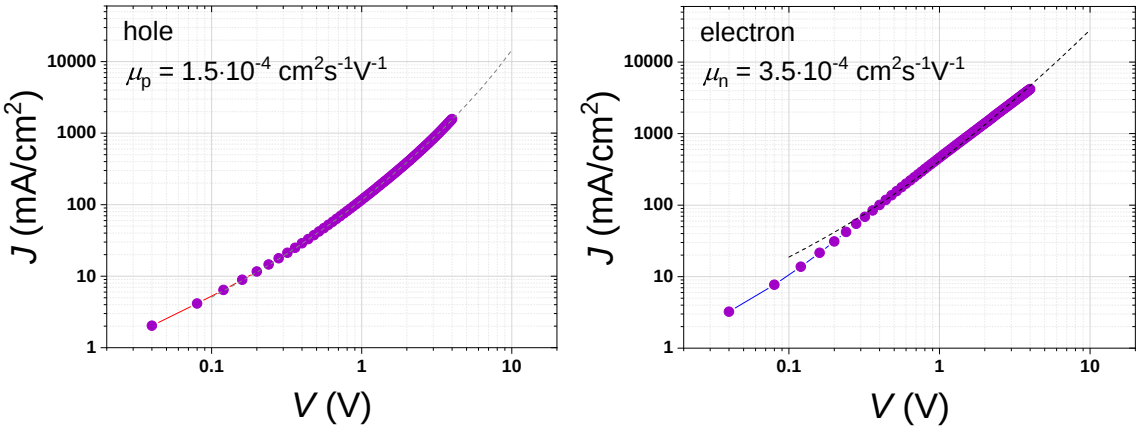

Figure S22: SCLC-plots of PPDT2FBT:Y6 hole and electron only diodes. Both diodes have a 100 nm thick active layer.

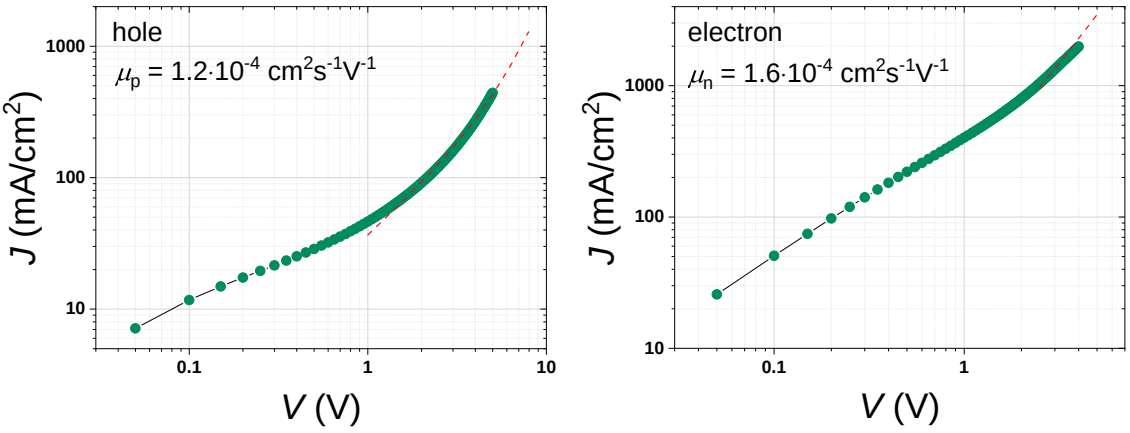

Figure S23: SCLC-plots of PM6:Y11 hole and electron only diodes. Both diodes have a 100 nm thick active layer.

References

[1] J. Vollbrecht, N. Tokmoldin, B. Sun, V. V. Brus, S. Shoaee, and D. Neher, "Determination of the charge carrier density in organic solar cells: A tutorial," *Journal of Applied Physics*, vol. 131, no. 22, p. 221 101, 2022.

[2] N. Tokmoldin *et al.*, "Explaining the fill-factor and photocurrent losses of nonfullerene acceptor-based solar cells by probing the long-range charge carrier diffusion and drift lengths," *Advanced Energy Materials*, vol. 11, no. 22, p. 2 100 804, 2021.

[3] N. Felekidis, A. Melianas, and M. Kemerink, "Automated open-source software for charge transport analysis in single-carrier organic semiconductor diodes," *Organic Electronics*, vol. 61, pp. 318–328, 2018.